Structural Changes of Horse Heart Ferricytochrome *c* Induced by Changes of Ionic Strength and Anion Binding[†]

Ronak Shah[‡,§] and Reinhard Schweitzer-Stenner*[,‡]

Department of Bioscience and Biotechnology, Drexel University, Philadelphia, Pennsylvania 19104

Received December 20, 2007; Revised Manuscript Received March 11, 2008

ABSTRACT: To test the validity of the notion that changes in ionic strength and ion binding do not cause any major functionally relevant structural changes in cytochrome *c*, we measured the absorption and electronic circular dichroism (ECD) of horse heart ferricytochrome *c* for the Soret and 695 nm charge-transfer band as a function of dihydrogen phosphate and sodium acetate concentrations. This band is known to probe the integrity of the functionally pivotal Fe^{3+}−M80 linkage. Spectral changes indicate that an ionic strength increase (via an increasing acetate ion concentration) affects only a subset of conformational substates of the Fe−M80 interface, probed by the 695 nm charge-transfer band, without a substantial modification of the heme environment. This result suggests that the substates probed by the 695 nm band differ with respect to their capability to transduce changes of solvent−protein interactions to the active site. The binding of $H_2PO_4^-$ ions causes more significant structural changes, which give rise to a large increase of the oscillator strength of the 695 nm band. This reflects a strengthening of the Fe−M80 bond in all substates, which probably destabilizes the oxidized state but stabilizes the folded state of the protein. Additional structural variations are likely to involve aromatic side chains, such as F82 and W59, and the hydrogen-bonding network in the heme pocket. In contrast to the current belief that anion binding to the binding domain of the protein for cytochrome *c* oxidase does not cause any functionally relevant structural changes, our results show that the structural variations that occur in the heme pocket are most likely of functional significance.

Cytochrome *c* is a small heme protein located in the intermembrane space of the mitochondria, where it mediates electron transfer from cytochrome *c* reductase to cytochrome *c* oxidase (*1*). This protein has been used extensively as a model to study electron-transport systems as well as protein folding (*1*−*4*). Many experiments, aimed at elucidating the relationship between structure and function of this molecule, have been performed at different, mostly rather high, ionic concentrations. Thus far, using different ionic strengths has not been considered a major problem, despite the fact that the redox potential decreases with an increasing ionic strength. Solution anions, such as HPO_4^{2-} and Cl^-, also affect the redox potential by modifying protein−solvent interactions and specific anion binding to positively charged patches on the protein surfaces, which partially neutralize the lowering of the redox potential caused by increasing the ion strength (*5, 6*). Structural changes of the protein are generally neglected in this context (*6*), because nuclear magnetic resonance (NMR)[1] and X-ray data seem to indicate the absence of any substantial changes of the structure of the protein by either varying the ionic strength or anion binding (*7, 8*). However, this perception overlooks the fact that side-chain conformations of specific amino acid residues depend upon the ionic strength of the medium (*7*). Feng et al. discovered some salt-dependent chemical-shift changes in the vicinity of residues 83−89 (*8*). According to Moench et al., there is a specific structural rearrangement with an increased ionic strength in the vicinity of the heme 3-CH_3 group, causing a decrease in the distance between the F82 B-CH_2 and the heme 3-CH_3 substituent (*9*). A significant expansion of the horse heart cytochrome *c* at low ionic strength and suppression at high ionic strength by small-angle X-ray scattering measurements was obtained by Trewhella et al. (*10*). Liu et al. used ultraviolet resonance Raman spectroscopy to detect that Tyr48 and Trp59 were affected by changing the ionic strength (*11*).

The current study was motivated by the consideration that structural changes related to ion strength and anion binding might be functionally relevant, even though they are comparatively small. A clarification of this issue could be of great relevance for a comprehensive understanding of the well-documented influence of the ionic strength and the anion concentration of the protein solution on the redox potential, conformational transitions of oxidized cytochrome *c* into non-native states, and the electron transfer between cytochrome *c* and cytochrome *c* oxidase (*5, 6, 12*). In this case, one would expect a significant influence on the Fe−M80 linkage, which is a major determinant of the redox potential of the protein

[†] Financial support to R.S.-S. was provided from the National Science Foundation (NSF) Grant MCB 0318749.

* To whom correspondence should be addressed: 3141 Chestnut Street, Philadelphia, PA, 19104. Telephone/Fax: 215-895-1265. E-mail: rschweitzer-stenner@drexel.edu.

[‡] Department of Chemistry.

[§] Department of Bioscience.

[1] Abbreviations: ECD, electronic circular dichroism; NMR, nuclear magnetic resonance; CT, charge transfer; SDS, sodium dodecyl sulfate; M80, methionine 80; H18, histidine 18; F82, phenylalanine 82; W59, tryptophan 59.

10.1021/bi702492n CCC: $40.75
Published on Web 04/12/2008

(*13*). In the model system microperoxidase 8, it accounts for 130 meV of the 410 meV energy gap between the reduced and oxidized states (*14*). To probe possible changes of this pivotal heme−protein interface, we measured the absorption and electronic circular dichroism (ECD) spectra of horse heart ferricytochrome *c* for the 695 nm (14.39×10^3 cm^{-1}) charge-transfer band as a function of sodium acetate and dihydrogen phosphate concentrations. Traditionally, the 695 nm band is assigned to an A_{2u}(porphyrin) → $d_{xz}(Fe^{3+})$ transition (*15*). Makinen and Churg proposed an E_g(heme) → $E_g(d_\pi)$ transition as an alternative assignment (*16*). However, these explanations do not account for the absence of the band in spectra of low-spin ferricytochrome *c* states, in which M80 is replaced by a ligand, such as lysine. McKnight et al. has proposed an alternative explanation, i.e., a S(M80) → Fe^{3+} transition, which would explain this observation (*17*). Its dependence on M80 as an axial ligand has made the band a frequently used tool to monitor conformational transitions of ferricytochrome *c* (*18*−*20*). Recent experiments in our laboratory have shown that the 695 nm band shape is asymmetric and composed of at least three subbands, which were assigned to different conformational substates (*20, 21*). These subbands are distinct from a second, weaker band at ca. 1200 cm^{-1} higher wavenumbers, which Eaton and Hochstrasser attributed to vibronic transitions (*15*).

We chose sodium acetate because the respective ions do not bind to horse heart cytochrome *c* up to a 0.2 M concentration (*5*), and therefore, variations of the concentration of the salt solely change the ionic strength. On the contrary, $H_2PO_4^-$, which at slightly acidic pH is the anion of a very common buffer, is likely to bind to the protein, such as the respective dianion HPO_4^{2-} (*7*). By comparing changes of the 695 nm band profile caused by increasing the concentrations of both salts, we are able to distinguish structural changes induced by ionic strength variations and anion binding. In what follows, the term 695 nm band is used as a designation of the considered charge-transfer band, whereas the results of the performed spectral decomposition are described in terms of wavenumber units.

MATERIALS AND METHODS

Horse heart cytochrome *c* was purchased from Sigma-Aldrich Co. (St. Louis, MO) and dissolved in potassium phosphate buffer and sodium acetate buffer to form a sample concentration of 5.0 mM. Different amounts of sodium acetate were added to 0.5 mM phosphate buffer solution of the protein to achieve various concentrations of acetate ions between 0.2 and 50 mM; the (mono) potassium phosphate buffer concentration was varied between 0.001 and 50 mM. The pH of the potassium phosphate buffer was adjusted to pH 6. A small amount of potassium ferricyanide (Fisher Scientific, Pittsburgh, PA) was added to oxidize the sample to eliminate traces of ferrocytochrome *c*, and subsequently, excess potassium ferricyanide was removed by dialysis. Using a JASCO J-810 spectropolarimeter purged with N_2, the 695 nm band was measured between 650 and 740 nm in a 1.0 mm quartz cell (Helma). A total of 15 accumulations were taken with a 5 nm bandwidth, a 500 nm/min scanning speed, and a 0.2 nm data pitch. For the final analysis, the background, taken with similar parameters, was subtracted with MULTIFIT.

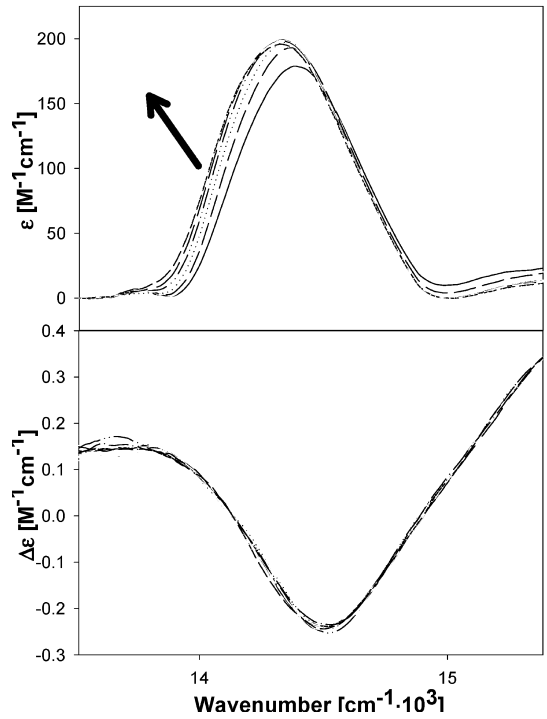

FIGURE 1: Absorption (top panel) and ECD (bottom panel) spectra for the 695 nm (14.39×10^3 cm^{-1}) charge-transfer band of horse heart ferricytochrome *c* measured at pH 7 (0.5 mM phosphate buffer) and varying sodium acetate concentrations (0.2, 0.3, 0.4, 0.5, 1, 2, 3, 4, 5, 20, 35, and 50 mM). The arrow indicates the changes with an increasing ionic strength.

RESULTS

As shown in Figure 1, increasing the acetate concentration causes a red shift and an increase in intensity on the low-energy side of the 695 nm absorption band. The total integrated intensity (and thus the oscillator strength) of the band increases concomitantly. Therefore, our results indicate that increasing the ionic strength causes the substates associated with the low-energy wing of the 695 nm band to gain oscillator strength, while the energy landscape of the Fe^{3+}−M80 linkage remains mostly unchanged. Contrary to the behavior of the absorption band, the corresponding ECD profile remains nearly unaffected by the increasing ionic strength (Figure 1). This is a very interesting and surprising result, because both, the absorption and ECD, depend upon the electronic dipole moments of the involved optical transition(s).

We subjected the absorption band to a self-consistent spectral decomposition, shown in Figure 2, for a low and high acetate concentration, by invoking a slightly modified version of the subband model reported by Dragomir et al. (*21*). The authors' model for a simultaneous fit of absorption and ECD profile comprised three central subbands located at 14.02×10^3 (S2), 14.36×10^3 (S3), and 14.70×10^3 cm^{-1} (S4), with Gaussian half-widths of 430, 510, and 730 cm^{-1}, respectively. To fit the absorption spectrum, the authors also included two additional side bands at 13.65×10^3 (S1) and 15.29×10^3 cm^{-1} (S5) to the low- and high-energy sides, respectively, whose appearance depends upon solution

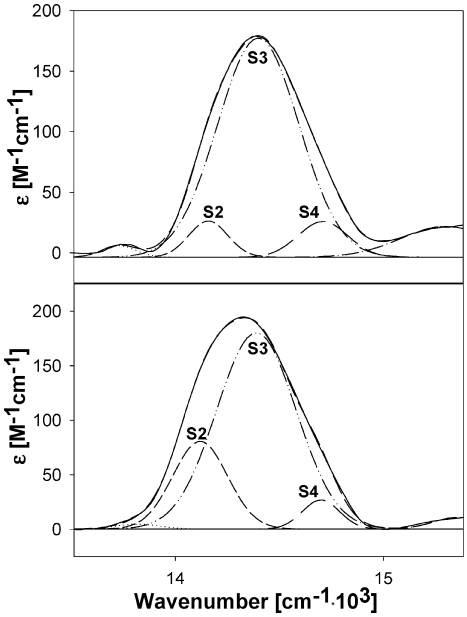

FIGURE 2: Self-consistent spectral decomposition of the charge-transfer absorption band measured at a low 0.2 mM (top panel) and a high 50 mM (bottom panel) sodium acetate concentration. The procedure is described in the text, and the obtained spectral parameters are listed in Table 1. The central subbands involved with the charge-transfer transition are labeled as S2, S3, and S4.

Table 1: Parameters from Spectral Decomposition[a]

	0.2 mM		50 mM	
subband	position (cm^{-1}, $\times 10^3$)	Gaussian half-width (cm^{-1}, $\times 10^3$)	position (cm^{-1}, $\times 10^3$)	Gaussian half-width (cm^{-1}, $\times 10^3$)
S1	13.73	0.19	13.82	0.25
S2	14.16	0.22	14.12	0.31
S3	14.40	0.46	14.39	0.45
S4	14.71	0.28	14.70	0.21
S5	15.30	0.51	15.36	0.28

[a] Parameter values were obtained from consistent spectral composition of the charge-transfer absorption band measured at a low (0.2 mM) and high (50 mM) sodium acetate concentration.

conditions. They might be assignable to other p(S) → d(Fe^{3+}) transitions (*17*). For S(6), one might follow Eaton and Hochstrasser by describing the band as a vibronic sideband reflecting interstate coupling with the Soret transition (*15*). However, recent experiments show that the intensity and profile of S(6) changes substantially if the protein is dissolved in a protein−glycerol mixture (Shah, Cupane, and Levantino, unpublished results). This observation is somewhat at variance with the proposed vibronic origin. The decomposition of the 695 nm absorption band measured at a low (0.2 mM) and high (50 mM) acetate concentration is shown in Figure 2, with the parameters detailed in Table 1. Figure 3 exhibits the effective oscillator strength f'

$$f'_j = \chi_j 9.2\times10^{-3}\int \varepsilon \, d\nu/\tilde{\nu}_{band} \qquad (1)$$

of the subbands S2−S4 as a function of the sodium acetate concentration, where f is expressed in D^2, j labels the subband, and $\tilde{\nu}_{band}$ is the wavenumber of the respective subband. The factor χ_j denotes the relative occupation of the jth substate with respect to the total manifold of substates involving the Fe−M bond. Only the intensity of the subband

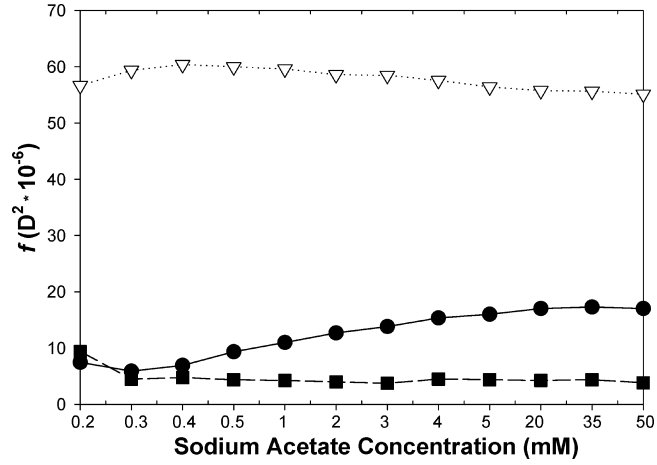

FIGURE 3: Oscillator strengths of the subbands of the charge-transfer absorption band as derived from a spectral decomposition plotted as a function of the sodium acetate concentration ionic strength. Only the subbands clearly assignable to the S(M80) → d(Fe^{3+}) charge-transfer transition are shown (S2, S3, and S4). S2 is graphed as filled circles on the solid line, while S3 is graphed as unfilled triangles on the short dashed line, and S4 is graphed as filled squares on the long dashed line.

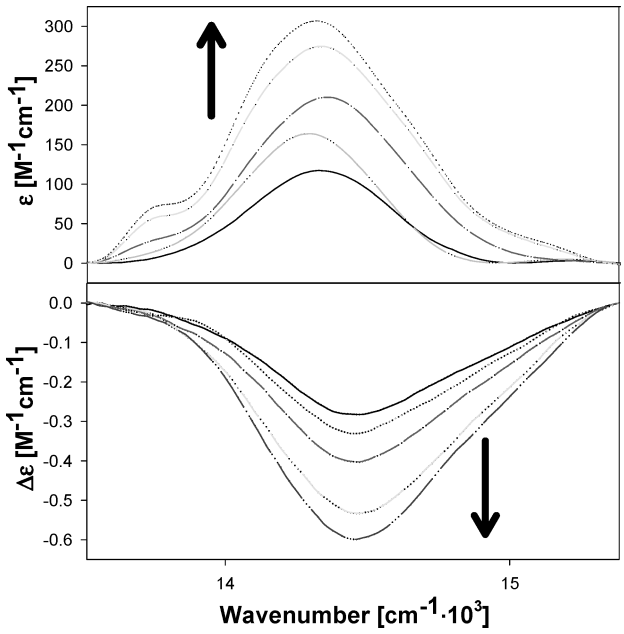

FIGURE 4: Absorption (top panel) and ECD (bottom panel) profiles of the 14.39 × 10^3 cm^{-1} charge-transfer band of horse heart ferricytochrome *c* measured at pH 6 and varying dihydrogen phosphate concentrations (0.5, 1, 5, 10, and 50 mM). The arrows indicate the changes with an increasing ionic strength.

(S2), associated with the low-energy wing of the 695 nm band profile, increases with rising ionic strength, while the intensities of the other subbands are practically independent of the salt concentration.

In contrast to what we observed for sodium acetate, the increase of the potassium phosphate buffer molarity substantially affects both the absorption and the ECD profile of the 695 nm band (Figure 4). The integrated intensities of both the absorption and ECD spectra increase substantially with a rising $H_2PO_4^-$ concentration, as indicated by the arrows in Figure 4. The subband model of Dragomir et al. (*21*) was again self-consistently employed. We applied a

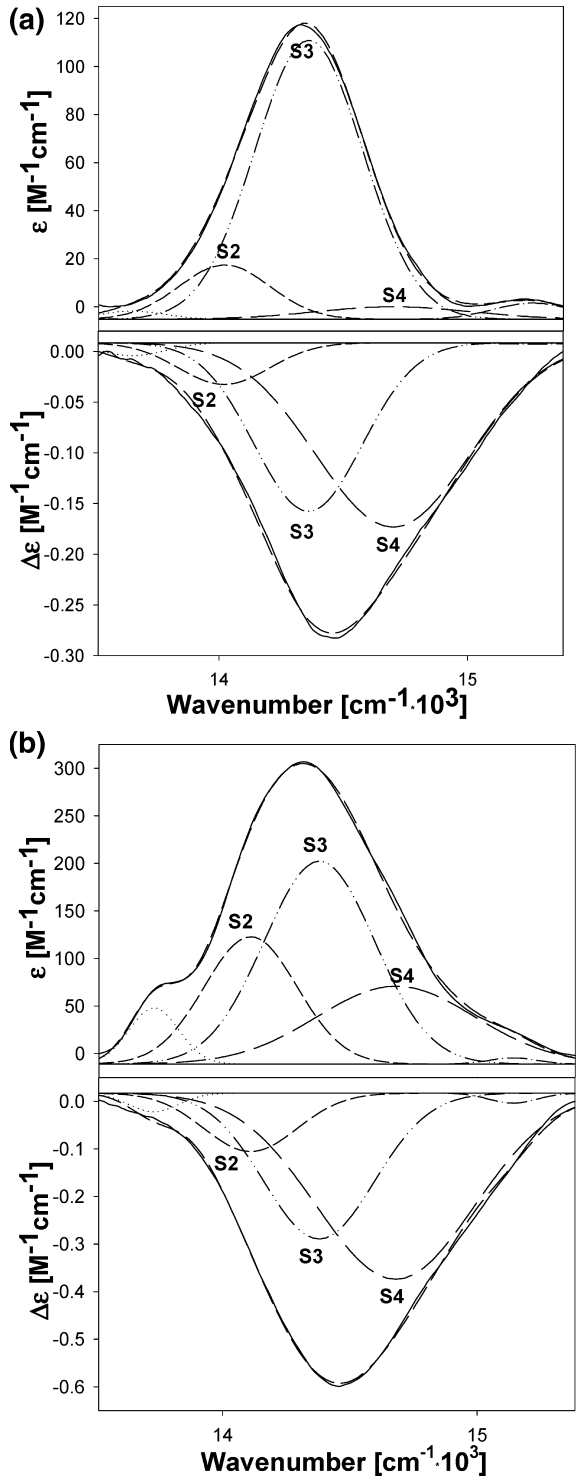

FIGURE 5: (a) Simultaneous spectral decomposition of the absorption (top panel) and ECD (bottom panel) profiles of the charge-transfer band measured at a low (0.5 mM) dihydrogen phosphate concentration. (b) Simultaneous spectral decomposition of the absorption (top panel) and ECD (bottom panel) profiles of the charge-transfer band measured at a high (50 mM) dihydrogen phosphate concentration. The procedure is described in the text, and the obtained spectral parameters are listed in Table 2. The central subbands involved with the charge-transfer transition are labeled as S2−S4.

simultaneous fit to the absorption and ECD profile at a low (0.5 mM) and high (50 mM) dihydrogen phosphate concentration as displayed in Figure 5, with the parameters detailed in Table 2. The spectral parameters of the three central subbands (wavenumbers and half-widths) that were originally assigned to the CT band by Dragomir et al. (*21*) are practically unchanged by the phosphate anion concentration.

Table 2: Parameters from Spectral Decomposition[a]

	0.5 mM		50 mM	
subband	position (cm^{-1}, $\times 10^3$)	Gaussian half-width (cm^{-1}, $\times 10^3$)	position (cm^{-1}, $\times 10^3$)	Gaussian half-width (cm^{-1}, $\times 10^3$)
S1	13.65	0.31	13.73	0.23
S2	14.02	0.43	14.11	0.43
S3	14.36	0.51	14.38	0.51
S4	14.70	0.73	14.68	0.73
S5	15.26	0.37	15.14	0.22

[a] Parameter values were obtained from simultaneous spectral decomposition of the absorption and ECD profile of the charge-transfer band measured at a low (0.5 mM) and high (50 mM) dihydrogen phosphate concentration.

Figure 6 exhibits the $H_2PO_4^-$ concentration dependence on the oscillator and rotational strengths of the subbands S2−S4. The latter has been calculated using

$$R'_j = \chi_j 2.3 \times 10^{-3} \int \Delta\varepsilon \, d\nu/\tilde{\nu}_{band} \qquad (2)$$

in units of D^2. Apparently, they all increase as a function of the anion concentration, although to a different extent. We also calculated the integrated Kuhn anisotropies (R/f) for the three subbands and plotted them as a function of the $H_2PO_4^-$ concentration, as shown in Figure 6.

We additionally measured the ECD spectrum of the B band of horse heart ferricytochrome c as a function of sodium acetate and $H_2PO_4^{-1}$ (Figure 7). As shown by Dragomir et al. (*21*), the observed couplet reflects B-band splitting, which can be predominantly attributed to the electric field in the heme pocket (*22*). An analysis based on the theory in reference (*23*) yielded a band splitting of about 500 cm^{-1} (Schweitzer-Stenner, unpublished). While the couplet remains nearly unaffected by the increasing sodium acetate concentration, the positive component gains intensity at the expense of the negative one with an increasing $H_2PO_4^{-1}$ concentration. The band splitting, however, remains constant.

DISCUSSION

Our results clearly show that both the increase of the ionic strength and anion binding to the protein surface affect the functionally pivotal Fe−M80 linkage, although to a different extent. The influence of ionic strength (varied by changing the sodium acetate concentration) on the structure-sensitive 695 nm band is modest, but the observed spectral changes are conspicuous, because the increase of the ionic strength affects only a part of the absorption spectra and does not change the ECD profile. We interpret this result as suggesting that additional oscillator strength is associated with polarizations that do not carry substantial rotational strength. The 695 nm band is known to be mostly z-polarized with some admixture of x and/or y polarization (*15*), which reflects the mixture of d_{xy}, d_{xz}, and d_{yz} orbitals by spin−orbit coupling and rhombic deformations (*17, 24*). The positions of absorption and ECD do not coincide, which clearly indicates that the band heterogeneity is associated with different mixtures of polarizations. If one assumes that the z polarization is mostly responsible for the rotational strength of the band, one arrives at the conclusion that the intensity additionally induced at high ionic strength is mostly x- or y-polarized.

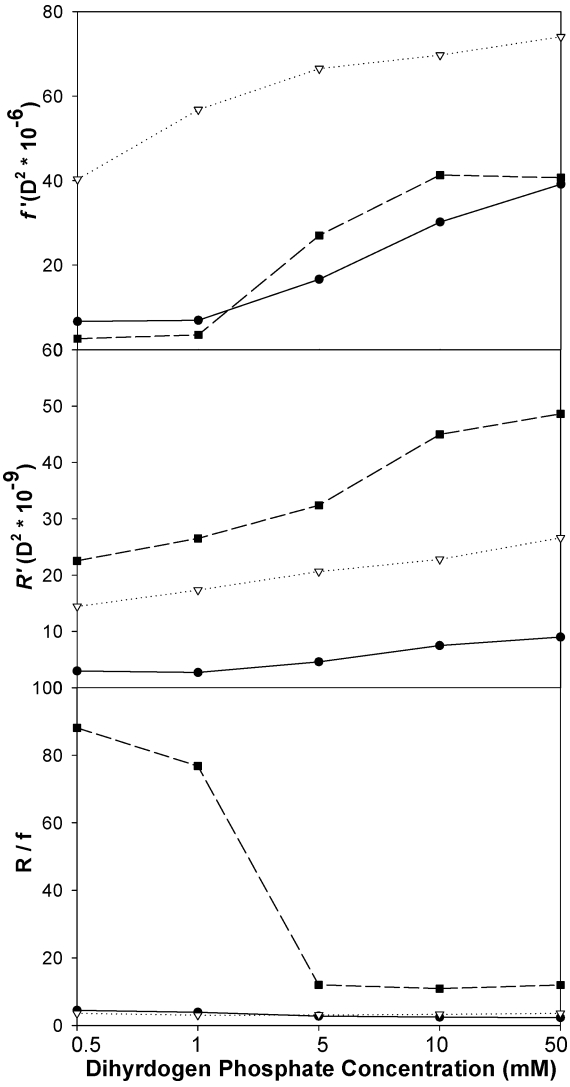

FIGURE 6: Integrated oscillator and rotational strengths of the subbands obtained from the spectral decomposition of the charge-transfer absorption (top panel) and ECD band (center panel), as well as the Kuhn anisotropy (bottom panel), plotted as a function of the dihydrogen phosphate concentration. Only the subbands clearly assignable to the S(M80) → d(Fe^{3+}) charge-transfer transition, S2−S4, are shown. S2 is graphed as filled circles on the solid line, while S3 is graphed as unfilled triangles on the short dashed line, and S4 is graphed as filled squares on the long dashed line.

Dragomir et al. (*21*) used the insights of Knight et al. (*17*) to interpret the 695 nm as resulting predominantly from a $p_y(S) \rightarrow d_{yz}(Fe^{3+})$ transition, which explains the *z* polarization. If this is correct, an *x*-polarized component would result from an admixture of the $p_y \rightarrow d_{xy}$ transition by spin−orbit coupling or electronic perturbations of *E* symmetry (*24*). Hence, our data suggest that the increase of the intensity of subband S2 reflects the presence of these perturbations, which could possibly be induced by a tilting of axial ligands.

A rising dihydrogen phosphate concentration causes the 695 nm absorption band to increase its oscillator strength, to broaden and become even more inhomogeneous. Generally, it is reasonable to assign an increase of the intensity of this band to a shorter distance between the Fe^{3+}−M80 bond. Our results therefore indicate that an increasing dihydrogen phosphate concentration causes a strengthening of the Fe−M80 linkage and concomitantly increases its conformational heterogeneity, owing to the fact that subbands S3 and S4 exhibit a stronger increase in their intensity than S2. Interestingly, the different response of the oscillator strength of the subbands to anion binding indicates that the substates have different anion-binding properties. For S2, the apparent binding constant is larger than 10^3 M^{-1}, whereas our data indicate binding affinities for S3 and S4 to be in the range of 10^{-2} to 2×10^2 M^{-1}. This estimation suggests that the substates are not localized but are involved with structural differences at the anion-binding sites.

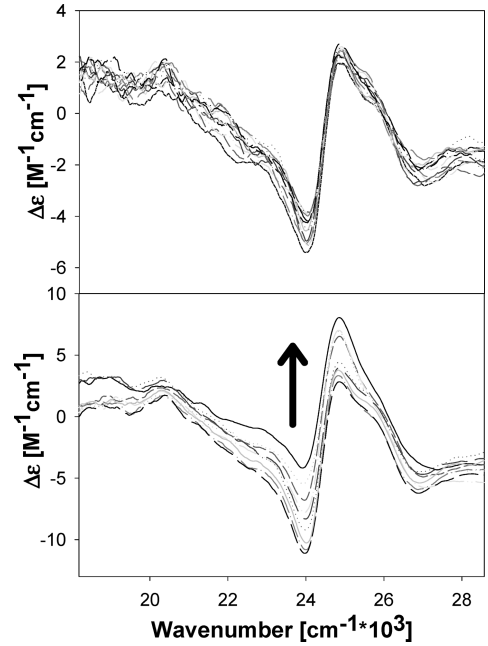

FIGURE 7: ECD of the Soret band of horse heart ferricytochrome *c* measured at varying sodium acetate (top panel) and dihydrogen phosphate (bottom panel) concentrations. The arrows indicate the changes with an increasing ionic strength.

The anion concentration dependences of the Kuhn anisotropies of the individual subbands are significantly different. This astonishing result provides conclusive evidence for the notion that the subbands are indeed related to different conformational substates and rule out a possible vibronic origin.

The Kuhn anisotropy can be written as

$$\frac{\Delta\varepsilon_j}{\varepsilon_j} = \frac{m_j \sin \vartheta_j}{\mu_j} \tag{3}$$

where m_j and μ_j denote the magnetic and electronic transition dipole matrix element associated with the 695 CT-subband *j* and ϑ is the angle between both dipole moments. $\mu_j \sim f_j'^{0.5}$ increases with an increasing anion concentration (upper panel in Figure 6) for all three subbands. For S4, which dominates the ECD band profile, the increase of μ_j accounts for most of the decreasing integrated Kuhn anisotropy. Interestingly, the corresponding Kuhn anisotropies of the other two substates S3 and S5 are practically independent of the anion concentration, despite a concomitant increase of the effective oscillator strength. This suggests that the magnetic and electronic moments in eq 3 exhibit nearly the same dependence upon anion binding. Alternatively, one may invoke a more complicated model by proposing that the increase of f'(S2) and f'(S4) reflects an increase of the relative fraction

of the respective substates. Because we do not observe any concomitant decrease of subband intensity, this would imply the existence of some additional substates, for which the 695 nm band has vanishing intensity. Further investigations will be necessary to clarify this issue.

It deserves to be mentioned in this context that resonance Raman spectroscopy has identified two different substates of the Fe−H18 linkage for the partially unfolded state of horse heart ferrocytochrome *c* in sodium dodecyl sulfate (SDS) (*25*). The heme was found to adopt a pentacoordinated state. The two substates were assigned to different strengths of hydrogen bonding between the N_δ of the proximal imidazole and neighboring D42 and P30 residues. Different strengths of these hydrogen bonds cause different strengths of Fe−H18 bonding and thus also modulate Fe−M80 bonding via the *trans* effect (*26*). Future experiments are needed to determine whether the heterogeneity of Fe−H18 in the ferrous state and Fe−M80 in the ferri state are really related.

The different influences of ionic strength and anion binding on the heme are also reflected by the ECD spectra of the B band shown in Figure 7 for dihydrogen phosphate and acetate ionic strength. ECD can be used to probe and quantify the splitting of B-band heme proteins, which do not appear in the absorption (*21, 27*). The ECD spectra yielded rotational strengths with opposite signs and different magnitudes for the B-state components, B_x and B_y. These components formed a couplet, with the band splitting being larger than the bandwidth. The couplet reflects band splitting, mostly because of electronic perturbations (*21, 23*), which result from the electric field in the heme cavity (*22*). The band splitting, however, is not changed by either acetate or dihydrogen phosphate ions, indicating that the internal electric field and its relative orientation remain unaffected. While the increase of the ionic strength does not cause any significant change of the ECD spectrum, anion binding of $H_2PO_4^-$ changes the shape of the couplet without affecting the respective splitting. This absence of change can be attributed to some orientational changes of chromophores, whose interaction with the heme induces the observed dichroism (*27, 28*). Leading candidates are the aromatic rings of F82 and W59, which are very close to the heme surface (*29*). F82 is part of the signal transduction pathway, which might transduce anion binding to the heme environment (*9*).

Overall, our results indicate that an ionic strength increase (via an increasing acetate ion concentration) selectively affects a subset of Fe^{3+}−M80 substates. This indication reveals that the different substates, probed by the 695 nm band, differ in terms of the strength of the solvent−heme coupling. This result is an important insight in view of the vital role in which solvent−protein interactions play in adjusting redox potential and reorganization energy, the two key parameters of the electron-transfer process (*5, 6*). Osherhoff et al. suggested that the high acetate concentration minimizes repulsion of like charges on the protein surface, thus strengthening hydrogen-bond interactions that are needed to maintain a closed structure in the heme crevice (*30*). Therefore, the protein contracts at high ionic strength, in agreement with small-angle X-ray scattering studies (*10*). A more compact structure certainly affects the functionally important hydrogen-bonding network in the heme cavity and thus also the geometry and strength of the Fe^{3+}−M80 linkage (*31*).

Apparently, the binding of $H_2PO_4^-$ to cytochrome *c* causes more significant structural changes, which involve a strengthening of the Fe−M80 bond. This is likely to decrease the enthalpy difference between the two oxidation states, which would stabilize the reduced state. However, the larger heterogeneity of the 695 nm band indicates a higher flexibility of the protein segment that contains M80. This flexibility should provide an entropic contribution to the Gibbs energy that favors the oxidized state. Doubtless, a stronger Fe−M80 bond increases the stability of the protein with respect to protein unfolding.

Structural studies of cytochrome *c* by Moench et al. revealed numerous positive-charged amino acid clusters on the surface of the protein that might function as binding sites (*8*). Pertaining to the chemical-shift changes, Feng et al. discovered in residues 83−89 the positively charged lysine residues at 86, 87, and 88 can act as a binding side for the phosphate anion (*7*). Additional structural variations might also involve F82 and the hydrogen-bonding network in the heme pocket (*8*). All of these residues belong to the conformationally very flexible Ω loop region constituted by residues 70−85 (*32*−*34*). The involvement of F82 in this loop region could explain the observed variation of the B-band couplet (*23*). These structural changes can involve residues that are part of the pathway, connecting the binding domain with the heme active site. It is noteworthy in this context that a recent study of Schweitzer-Stenner et al. (*20*) revealed that the temperature dependence of the 695 nm band shows a biphasic behavior. In addition to its bleaching at temperatures above 50 °C, the total intensity of the band increases from a plateau between 10 and 40 °C toward subzero temperatures. This result was interpreted as the population of another, yet unexplored protein state. It is reasonable to conclude that our data indicate an upshift of the respective transition temperature with increasing $H_2PO_4^-$ ions, causing it to become populated at room temperature. This is consistent with the fact that anion binding increases the apparent p*K* value of the transition between the native state III and the alkaline state IV, which reflects a stabilization of the native state and thus most likely also the Fe−M80 bond (*12*).

Our results parallel, to some extent, recent observations on cytochrome *c*−cardiolipin complexes in 1,2-dioleoyl-*sn*-glycero-3-phosphocholine liposomes by Belikova et al. (*35*). The binding to cardiolipin, which serves as a substrate for cytochrome *c*, substantially reduces the 695 nm band of the ferri state by ca. 60% at low anion concentrations. This effect can be completely eliminated by adding 1 M KCl^-. Similar to phosphate ions, Cl^- binds to positively charged patches on the protein surface (*6*).

It should be mentioned in this context that the above-discussed structural variations can only partially account for the experimentally obtained changes of the redox potential caused by anion binding, which causes a decrease of the potential at low (zero) and an increase of the potential at high ionic strengths, thus substantially reducing its ionic strength dependence (*6, 36*). As discussed in detail by Battistuzzi et al., the neutralization of charges on the protein surface by bound anions alters the

electrostatic interactions, which contribute to the Gibbs energy associated with the redox potential (*6*). While this purely electrostatic effect is certainly relevant, the structural changes elucidated in the current study cannot be negligible in view of the fact that the observed changes of the 695 nm band oscillator strength must be considered as large.

When our data are taken together, they provide strong evidence that the small-scale structural changes, caused by differences in ionic strength and anion binding to the protein surface, involve substantial structural variations of the $Fe^{3+}-M80$ bond, which is one of the key determinants of the redox potential. Therefore, these changes cannot be dismissed as irrelevant. Our study, rather, suggests that a thorough understanding of functionally relevant modes of protein−solvent interactions requires an assessment of the conformational heterogeneity and dynamics of those parts of the protein, which transduce these interactions. Our results further point to the necessity to elucidate the relationship between the charge-transfer band and the structural properties of the Fe−M80 linkage. Finally, the results lead to the recommendation that spectroscopic and functional studies of oxidized cytochrome *c* can only be related to each other if they were carried out at the same solvent conditions.

ACKNOWLEDGMENT

We thank Andrew Hagarman for critically reading the manuscript.

REFERENCES

1. Moore, G. W., and Pettigrew, G. W. (1990) *Cytochrome c's Evolutionary, Structural and Physicochemical Aspects*, Springer, Berlin, Germany.
2. Lyubovitsky, J. G., Gray, H. B., and Winkler, J. R. (2002) Mapping the cytochrome *c* folding landscape. *J. Am. Chem. Soc. 124*, 5481–5485.
3. Pletneva, E. V., Gray, H. B., and Winkler, J. R. (2005) Snapshots of cytochrome *c* folding. *Proc. Natl. Acad. Sci. U.S.A. 102*, 18397–18402.
4. Latypov, R. F., Cheng, H., Roder, N., Zhang, A., and Roder, H. (2006) Structural characterization of an equilibrium unfolding intermediate in cytochrome *c*. *J. Mol. Biol. 357*, 1009–1025.
5. Battistuzzi, G., Loschi, L., Borsari, M., and Sola, M. (1999) Effects of nonspecific ion−protein interactions of the redox chemistry of cytochrome *c*. *J. Biol. Inorg. Chem. 4*, 601–607.
6. Battistuzzi, G., Borsari, M., Dallari, D., Lancellotti, I., and Sola, M. (1996) Anion binding to mitochondrial cytochromes *c* studied through electrochemistry. Effects of the neutralization of surface charges on the redox potential. *Eur. J. Biochem. 241*, 208–214.
7. Sanishvili, R., Volz, K. W., Westbrook, E. M., and Margoliash, E. (1995) The low ionic strength crystal structure of horsed cytochrome *c* at 2.1 Å resolution and comparison with its high ionic strength counterpart. *Structure 3*, 707–716.
8. Feng, Y., and Englander, S. W. (1990) Salt-dependent structure change and ion binding in cytochrome *c* studied by two-dimensional proton NMR. *Biochemistry 29*, 3505–3509.
9. Moench, S. J., Shi, T., and Satterlee, J. D. (1991) Proton-NMR studies of the effects of ionic strength and pH on the hyperfine-shifted resonances and phenylalanine-82 environment of three species of mitochondrial ferricytochrome *c*. *Eur. J. Biochem. 197*, 631–641.
10. Trewhella, J., Carlson, V., Curtis, E. H., and Heidorn, D. B. (1988) Differences in the solution structures of oxidized and reduced cytochrome *c* measured by small-angle X-ray scattering. *Biochemistry 27*, 1121–1125.
11. Liu, G., Grygon, C. A., and Spiro, T. G. (1989) Ionic strength dependence of cytochrome *c* structure and Trp-59 H/D exchange from ultraviolet resonance Raman spectroscopy. *Biochemistry 28*, 5046–5050.
12. Battistuzzi, G., Borsari, M., Ranieri, A., and Sola, M. (2001) Effects of specific anion−protein binding on the alkaline transition of cytochrome *c*. *Arch. Biochem. Biophys. 386*, 117–122.
13. Silkstone, G. G., Cooper, C. E., Svistunenko, D., and Wilson, M. T. (2005) EPR and optical spectroscopic studies of Met80X mutants of yeast Ferricytochrome *c*. Models for intermediates in the alkaline transition. *J. Am. Chem. Soc. 127*, 92–99.
14. Tezcan, F. A., Winkler, J. R., and Gray, H. B. (1998) Effects of ligation and folding on reduction potentials of heme proteins. *J. Am. Chem. Soc. 120*, 13383–13388.
15. Eaton, W., and Hochstrasser, R. M. (1968) Single crystal spectra of ferricytochrome *c*. *J. Chem. Phys. 49*, 985–995.
16. Makinen, M. V., and Churg, A. K. (1983) Structural and analytical aspects of the electronic spectra of hemeproteins, in *Iron Porphyrins*, Vol. 1, pp 141−235 (Lever, A. B. P., and Gray, H., Eds.) Addison and Wesley, Reading, U.K.
17. McKnight, J., Cheesman, M. R., Thomson, A. J., Miles, J. S., and Munro, A. W. (1993) Identification of the charge transfer transitions in the optical spectrum of low-spin ferri-cytochrome P-450 *Bacillus megaterium*. *Eur. J. Biochem 213*, 683–687.
18. Schejter, A., and George, P. (1964) The 695 μm band of ferricytochrome *c* and its relationship to protein conformation. *Biochemistry 3*, 1045–1049.
19. Kaminsky, L. S., Miller, V. L., and Davison, A. J. (1973) Thermodynamic studies of the heme crevice of ferrocytochrome *c*. *Biochemistry 12*, 2215–2221.
20. Schweitzer-Stenner, R., Shah, R., Hagarman, A., and Dragomir, I. (2007) Conformational substates of horse heart cytochrome *c* exhibit different thermal unfolding of the heme cavity. *J. Phys. Chem. B 111*, 9603–9607.
21. Dragomir, I., Hagarman, A., Wallace, C., and Schweitzer-Stenner, R. (2007) Optical band splitting and electronic perturbations of the heme chromophore in cytochrome *c* at room temperature probed by visible electronic circular dichroism spectroscopy. *Biophys. J. 92*, 989–998.
22. Manas, E. S., Vanderkooi, J. M., and Sharp, K. A. (1999) The effects of protein environment on the low temperature electronic spectroscopy of cytochrome *c* and microperoxidase-11. *J. Phys. Chem. 103*, 6344–6348.
23. Schweitzer-Stenner, R, Gorden, J. P., and Hagarman, A. (2007) The asymmetric band profile of the Soret band of deoxymyoglobin is caused by electronic and vibronic perturbations of the heme group rather than by a doming deformation. *J. Chem. Phys. 127*, 135103.
24. Salmeen, I., and Palmerand, G. (1968) Electron paramagnetic resonance of beef-heart ferricytochrome *c*. *J. Chem. Phys. 48*, 2049–2052.
25. Droghetti, E., Oellerich, S., Hildebrandt, P., and Smulevich, G. (2006) Heme coordination states of unfolded ferrous cytochrome *c*. *Biophys. J. 91*, 3022–3031.
26. Marti, M. A., Scherlis, D. A., Doctorovich, F. A., Ordejón, P., and and Estrin, D. A. (2003) Modulation of the NO trans effect in heme proteins: Implications for the activation of soluble guanylate cyclase. *J. Biol. Inorg. Chem. 8*, 595–600.
27. Hsu, M., and Woody, R. W. (1971) The origin of the heme cotton effects in myoglobin and hemoglobin. *J. Am. Chem. Soc. 93*, 3515–3525.
28. Blauer, G., Sreeama, N., and Woody, R. W. (1993) Optical activity of hemoproteins in the Soret region. Circular dichroism of the heme undecapeptide of cytochrome *c* in aqueous solution. *Biochemistry 32*, 66774–6679.
29. Berghuis, A. M., and Brayer, G. D. (1992) Oxidation state-dependent conformational changes in cytochrome *c*. *J. Mol. Biol. 223*, 959–976.
30. Osherhoff, N., Borden, D., Koppenol, W. H., and Margoliash, E. (1980) Electrostatic interactions in cytochrome *c*. The role of interactions between residues 13 and 90 and residues 79 and 47 in stabilizing the heme crevice structure. *J. Biol. Chem. 255*, 1689–1697.
31. Berghuis, A. M., Guillemette, J. G., McLendon, G., Sherman, F., Smith, M., and Brayer, G. D. (1994) Mutation of tyrosine-67 to phenylalanine in cytochrome *c* significantly alters the local heme environment. *J. Mol. Biol. 236*, 786–799.
32. Margoliash, E., and Schejter, A. (1966) Cytochrome *c*. *Adv. Protein Chem. 21*, 113–286.

33. Englander, S. W., Sosnick, T. R., Mayne, L. C., Shtilerman, M., Phoebe, X. Q., and Bai, Y. (1998) Fast and slow folding in cytochrome *c*. *Acc. Chem. Res. 31*, 737–744.
34. Krishna, M. M. G., Maity, H., Rumbley, J. N., Lin, Y., and Englander, S. W. (2006) Order of steps in the cytochrome *c* folding pathway: Evidence for a sequential stabilization mechanism. *J. Mol. Biol. 359*, 1410–1419.
35. Belikova, N. A., Vladimirov, Y. A., Osipov, A. N., Kapralov, A. A., Tyurin, V. A., Potapovich, M. V., Basova, L. V., Peterson, J., Kurnikov, I. V., and Kagan, V. E. (2006) Peroxidase activity and structural transitions of cytochrome *c* bound to cardiolipin-containing membranes. *Biochemistry 45*, 4998–5009.
36. Battistuzzi, G., Borsari, M., and Sola, M. (2001) Medium and temperature effects on the redox chemistry of cytochrome *c*. *Eur. J. Inorg. Chem.* 2889–3004.

BI702492N